

Mode-locked laser with multiple timescales in a microresonator-based nested cavity

Original

Mode-locked laser with multiple timescales in a microresonator-based nested cavity / Aadhi, A.; Alamgir, Imtiaz; Di Lauro, Luigi; Fischer, Bennet; Perron, Nicolas; Dmitriev, Pavel; Mazoukh, Celine; Roztock, Piotr; Rimoldi, Cristina; Chemnitz, Mario; Eshaghi, Armaghan; Viktorov, Evgeny A.; Kovalev, Anton V.; Little, Brent E.; Chu, Sai T.; Moss, David J.; Morandotti, Roberto. - In: APL PHOTONICS. - ISSN 2378-0967. - ELETTRONICO. - 9:3(2024), pp. 1-8. [10.1063/5.0174697]

Availability:

This version is available at: 11583/2987676 since: 2024-04-09T08:50:55Z

Publisher:

AIP Publishing

Published

DOI:10.1063/5.0174697

Terms of use:












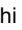






This article is made available under terms and conditions as specified in the corresponding bibliographic description in the repository

Publisher copyright

(Article begins on next page)

LETTER | MARCH 01 2024

Mode-locked laser with multiple timescales in a microresonator-based nested cavity

A. Aadhi ; Imtiaz Alamgir ; Luigi Di Lauro  ; Bennet Fischer ; Nicolas Perron ; Pavel Dmitriev ; Celine Mazoukh ; Piotr Roztocki ; Cristina Rimoldi ; Mario Chemnitz ; Armaghan Eshaghi ; Evgeny A. Viktorov ; Anton V. Kovalev ; Brent E. Little ; Sai T. Chu ; David J. Moss ; Roberto Morandotti 



APL Photonics 9, 031302 (2024)

<https://doi.org/10.1063/5.0174697>



Biomicrofluidics
Special Topic:
Microfluidic Biosensors
Submit Today



Mode-locked laser with multiple timescales in a microresonator-based nested cavity

Cite as: APL Photon. 9, 031302 (2024); doi: 10.1063/5.0174697

Submitted: 1 September 2023 • Accepted: 4 January 2024 •

Published Online: 1 March 2024



A. Aadhi,¹ Imtiaz Alamgir,¹ Luigi Di Lauro,^{1,a)} Bennet Fischer,² Nicolas Perron,¹ Pavel Dmitriev,¹ Celine Mazoukh,¹ Piotr Roztocki,^{1,3} Cristina Rimoldi,⁴ Mario Chemnitz,^{1,2} Armaghan Eshaghi,⁵ Evgeny A. Viktorov,⁶ Anton V. Kovalev,⁶ Brent E. Little,⁷ Sai T. Chu,⁸ David J. Moss,⁹ and Roberto Morandotti¹

AFFILIATIONS

¹ Institut National de la Recherche Scientifique-Énergie Matériaux Télécommunications, 1650 Boulevard Lionel Boulet, Varennes, Quebec J3X 13, Canada

² Leibniz Institute of Photonic Technology, Albert-Einstein Str. 9, 07745 Jena, Germany

³ Ki3 Photonics Technologies, 2547 Rue Sicard, Montreal, Quebec H1V 2Y8, Canada

⁴ Dipartimento di Elettronica e Telecomunicazioni, Politecnico di Torino, Corso Duca degli Abruzzi 24, 10129 Torino, Italy

⁵ Huawei Technologies Canada, 19 Allstate Parkway, Markham, Ontario L3R 5A4, Canada

⁶ ITMO University, Birzhnevaya Liniya 14, 199034 St. Petersburg, Russia

⁷ QXP Technology Inc., Xi'an, Shaanxi 710119, China

⁸ City University of Hong Kong, Tat Chee Avenue, Hong Kong, China

⁹ Optical Sciences Centre, Swinburne University of Technology, Hawthorn, Vic 3122, Australia

Note: This paper is part of the APL Photonics Special Topic on State-of-the-Art and Future Directions in Optical Frequency Comb Sources, Enabling Technologies, and Applications.

^{a)} **Authors to whom correspondence should be addressed:** Imtiaz.Alamgir@inrs.ca, Luigi.DiLauro@inrs.ca, and Roberto.Morandotti@inrs.ca

ABSTRACT

Mode-locking techniques have played a pivotal role in developing and advancing laser technology. Stable fiber-cavity configurations can generate trains of pulses spanning from MHz to GHz speeds, which are fundamental to various applications in micromachining, spectroscopy, and communications. However, the generation and exploitation of multiple timescales in a single laser cavity configuration remain unexplored. Our work demonstrates a fiber-cavity laser configuration designed to generate and control pulse trains from nanosecond to picosecond timescales with a broadband output and a low mode-locking threshold. Our approach exploits a frequency mode-locking mechanism that simultaneously drives the modes of an integrated microring resonator nested within an external fiber-loop cavity, guaranteeing ultra-stable operation. By selectively filtering the nested cavity modes, we can transition from nanosecond pulses to pulse burst trains in which nanosecond and picosecond components coexist. Our laser configuration produces a train of pulses with durations of 5.1 ns and 3.1 ps at repetition rates of 4.4 MHz and 48.7 GHz, with time-bandwidth products close to the transform-limited values of 0.5 and 0.46, respectively. Moreover, in the absence of frequency modulation, we demonstrate the generation of comb spectra with an adjustable central wavelength. Our findings have the potential to significantly contribute to the development of cutting-edge technologies and applications, harnessing the distinct advantages of mode-locked pulses across various scientific and engineering disciplines.

© 2024 Author(s). All article content, except where otherwise noted, is licensed under a Creative Commons Attribution (CC BY) license (<http://creativecommons.org/licenses/by/4.0/>). <https://doi.org/10.1063/5.0174697>

I. INTRODUCTION

Mode-locking techniques synchronize the phases of multiple longitudinal laser modes to generate robust and stable optical pulse trains. The repetition rates (REPs) of pulse trains can vary from MHz to GHz in fiber cavity configurations,^{1–3} providing versatile platforms with robust designs and broad transmission windows. These have significantly contributed to technological advancements in telecommunications, precision measurements, quantum entanglement,^{4–9} and neuromorphic computing.^{10–13} Mode-locking operation is achieved by tailoring cavity loss through active⁷ and passive¹ modulation techniques, where various parameters, including pump power, polarization, cavity configuration, and dispersion,^{14,15} influence the generated pulse properties.

Passive mode-locking has been demonstrated using various saturable absorbers made of graphene and carbon nanotubes, as well as through nonlinear integrated devices such as spiral waveguides^{3,16} and integrated microring resonators (MRRs),^{17–19} resulting in compact and efficient laser architectures.^{20–23} Picosecond mode-locked pulses can be generated, e.g., in figure-eight¹⁸ and nested-cavity laser configurations,^{17,24} with REPs in the 50–400 GHz range.²⁵

We note that such schemes suffer from thermo-optical effects and phase fluctuations²⁶ that impact their stability. Moreover, they require spectral filtering to select the desired cavity mode resonance, which drastically increases the mode-locking threshold, reduces bandwidth, and introduces significant experimental complexity. On the other hand, the generation of nanosecond pulses through passive mode-locking techniques is hindered by the challenge of balancing the power threshold required for nonlinear effects on short timescales against the response of slower, saturable absorbers. Furthermore, the implementation of lengthy nanosecond cavities introduces significant chirps²⁶ and relatively lower peak powers, in turn requiring intricate compensation techniques that limit their applicability.

Active mode-locking techniques can generate pulses with durations between hundreds of nanoseconds and a few picoseconds.^{25,27} This is generally achieved by modulating the phase, frequency, or amplitude of the optical intracavity fields through electro-/acousto-optic modulators. While requiring additional radiofrequency (RF) components, actively mode-locked lasers benefit from a reduced power threshold and the absence of undesirable nonlinear optical effects (e.g., thermo-optical²⁸). Similarly to the case of passive schemes, fiber cavities with nested MRRs represent a suitable configuration for nanosecond pulse generation through the realization of active mode-locked lasers.⁷ Nevertheless, the simultaneous generation of slow and fast dynamics in a single laser configuration, ranging from nanosecond to picosecond timescales, remains unexplored.

In this work, we demonstrate a mode-locked laser featuring an MRR nested in an external fiber-cavity configuration actively driven by an intracavity phase modulator (PM), allowing for laser operations characterized by the presence of multiple timescales. We report the presence of nanosecond pulses and regular pulse burst trains with nanosecond and picosecond components. By selectively filtering the MRR resonances using an external cavity filter, we can switch between different timescales and significantly reduce

the intracavity pump power, hence the mode-locking threshold. The dynamical control of laser operations through an adjustable filter-driven mechanism^{24,29,30} underscores the tunability and versatility of our system. The laser cavity is stabilized by applying a frequency-modulated (FM) electronic signal to the PM, establishing a fixed phase relationship between the external cavity modes and the MRR resonances. Furthermore, in the absence of modulation, our approach provides the added benefit of directly tuning the central wavelength of the generated frequency comb—a capability lacking in traditional actively mode-locked lasers, where wavelength adjustment necessitates precise frequency modulation readjustment. In such a mode of operation, we demonstrate the generation of frequency combs with a tunable central wavelength spanning from 1.530 to 1.562 μm . This still represents a challenge for other wave-length tuning techniques involving mechanical,³¹ electro,³² or thermo-optical effects.³³

Our technique holds promises for numerous applications, such as micromachining^{34,35} and the realization of a pump source for mid-infrared pulse generation.³⁶ At the same time, the realization of GHz microcombs finds applications in ultra-fast precision spectroscopy,³⁷ metrology,^{38,39} coherent communication,⁴⁰ and optical computing.¹⁰

II. EXPERIMENTAL IMPLEMENTATION

Figure 1 illustrates the experimental setup of our scheme. This configuration employs an integrated CMOS-compatible high-Q ($Q = 0.8 \times 10^6$) MRR, which is made of a high-index glass (refractive index $n = 1.6$) buried in silica with a cross section of $3 \mu\text{m} \times 2 \mu\text{m}$. The high nonlinear coefficient ($\gamma \sim 200 \text{ W}^{-1} \text{ km}^{-1}$) of the MRR is associated with the Kerr nonlinearity as well as with low linear ($\sim 0.06 \text{ dB/cm}$) and negligible nonlinear propagation losses. The MRR has a ring radius of $593 \mu\text{m}$, a free-spectral range of $F_{\text{MRR}} = 48.7 \text{ GHz}$, and a resonance linewidth of 100 MHz .⁴¹ The group velocity dispersion of the MRR is $\beta_2 \sim -3 \text{ ps}^2 \text{ km}^{-1}$ and $\beta_2 \sim -10 \text{ ps}^2 \text{ km}^{-1}$ at 1550 nm for the TM and TE modes, respectively, both featuring anomalous dispersion profiles around the wavelength range considered in our experiments.⁴² The input and output bus waveguides of the MRR are pigtailed to standard single-mode fibers via integrated mode converters employing V-groove technology. The MRR, depicted in Fig. 1, is thermally stabilized using a thermoelectric controller with a feedback circuit to prevent thermal fluctuations. This platform is nested in an external fiber-cavity, which also includes an erbium-doped fiber amplifier (EDFA, maximum gain of 30 dB over the telecom C-band) from Keopsys Industries as the gain medium; a frequency tunable (C-band) Santec 950 optical filter with adjustable bandwidth up to 6 nm ; a polarization maintaining isolator, and a polarization controller. The tunable passband filter selects specific MRR resonances contributing to different laser regimes. The total optical length of the external fiber cavity is $\sim 45.8 \text{ m}$, corresponding to a free-spectral range of $F_{\text{ext}} = 4.4 \text{ MHz}$. Therefore, a maximum number of ~ 22 external cavity modes can oscillate within each single MRR resonance. A 40 GHz bandwidth PM (EO Space, X-cut, and low half-wave voltage), driven by an RF synthesizer (Rohde and Schwarz, tunable bandwidth from 2 to 40 GHz), sustains an FM signal with a 4.4 MHz modulation frequency locked to a carrier with a frequency of 24.35 GHz and a linewidth in the range of a few tens of KHz. The latter, in turn, actively phase-locks the external cavity

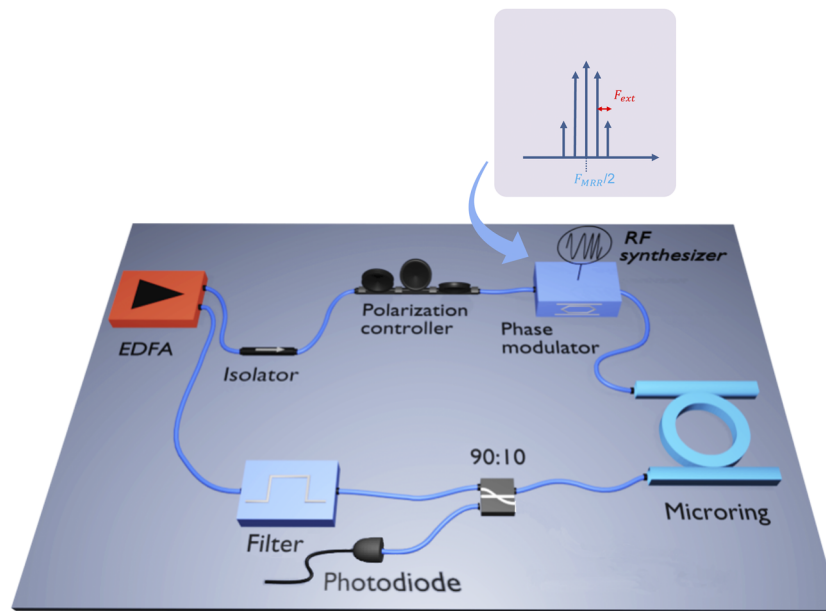


FIG. 1. Experimental schematic of the mode-locking laser. The experimental setup comprises an EDFA (erbium-doped fiber amplifier), a PC (polarization controller), a PM (phase modulator) with a bandwidth of 40 GHz, a PD (photodiode), an RF (radio-frequency) synthesizer with a tunable bandwidth ranging from 2 to 40 GHz, and an MRR (microring resonator) characterized by a nonlinear coefficient $\gamma \sim 200 \text{ W}^{-1} \text{ km}^{-1}$ and linear losses of $\sim 0.06 \text{ dB/cm}$. For thermal stability, the MRR is mounted on a thermoelectric controller (not shown). The EDFA plays a crucial role in sustaining the lasing of the external cavity modes featuring a free-spectral range of $F_{ext} = 4.4 \text{ MHz}$, specifically within the resonances of the MRR, whose free-spectral range (F_{MRR}) is 48.7 GHz. These MRR resonances act as filters, restricting the number of external modes allowed to oscillate in the laser. The tunable filter can select a variable number of MRR resonances within its bandwidth. The upper inset in the figure schematically illustrates the RF spectrum of the frequency-modulated signal that establishes a fixed phase relationship among all adjacent oscillation modes within multiple MRR modes.

and the MRR modes to the RF signal. The polarization controller sets the polarization in either the transverse magnetic or electric modes of the MRR, whose zero dispersion wavelengths are in the C-band and L-band, respectively.⁴³ A 10% portion of the intracavity field is extracted from the cavity for spectral and temporal analysis via an Ando AQ6317B optical spectrum analyzer (OSA), a photodiode (40 GHz bandwidth), an oscilloscope (Agilent Dso-x 92804A, 28 GHz bandwidth), an electrical RF spectrum analyzer (HP E4407B, 25 GHz bandwidth), and an optical sampling scope (Exfo PSO-10, 500 GHz bandwidth).

III. RESULTS AND DISCUSSION

The presence of the EDFA in the external cavity sustains the lasing of the external cavity modes that oscillate within the MRR resonances while filtering out the other external modes. The low anomalous dispersion of the MRR ($<10 \text{ ps}^2 \text{ km}^{-1}$) results in a negligible parametric phase-mismatch among these external cavity modes and induces highly efficient stimulated four-wave mixing (FWM),^{44,45} effectively broadening the overall spectral bandwidth of the frequency comb. However, the random beating between many external cavity modes within the MRR resonances leads to unstable operation without a mechanism that locks their phases. Therefore, it is essential to actively modulate both the external cavity and the MRR modes to ensure that a phase-locking condition is satisfied for the modes within each resonance and between the MRR resonances.

Since the analog bandwidths of the PM and the RF synthesizer are limited to 40 GHz, we set the signal modulation to operate at a sub-harmonic of F_{MRR} , which is 24.35 GHz. Consequently, each successive pair of generated tones aligns with the F_{MRR} , while the spacing between the modulation components resonating inside the external laser cavity is equal to 4.4 MHz. When the filter bandwidth is 100 GHz, i.e., allowing the external cavity modes of two MRR resonances to oscillate, mode-locked pulse burst trains emerge with coexisting nanosecond and picosecond timescales. The simultaneous locking of both cavity modes, which produces dynamics with different timescales, is a crucial mechanism of our scheme. This overall process is schematically depicted in Fig. 2. The pulse burst trains present nanosecond components with a REP matching the external cavity free-spectral range $F_{ext} = 4.4 \text{ MHz}$. The temporal profile is Gaussian with a 5.1 ns width, as shown in Figs. 3(a) and 3(b). This produces a transform-limited time-bandwidth product of 0.5, considering that the MRR resonance is $\sim 100 \text{ MHz}$. Figure 3(c) depicts highly coherent RF spectral components with 4.4 MHz spacing, measured by an electrical RF spectrum analyzer (25 GHz bandwidth). This indicates phase-locking among all the distinct external cavity modes oscillating inside the MRR resonances. The inset in Fig. 3(c) illustrates a measured linewidth of 2.9 kHz for the fundamental RF tone, indicating the high stability of the laser REP. Figures 3(a)–3(c) depict the nanosecond timescale characterization of the mode-locked regime with two MRR resonances within the external filter bandwidth. The temporal and spectral profiles are

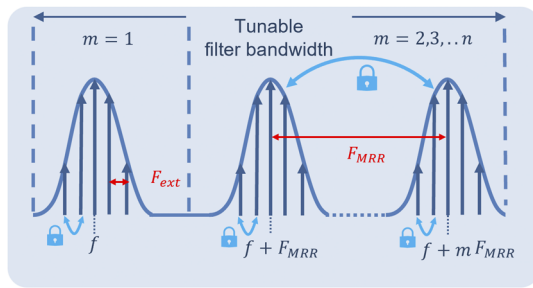


FIG. 2. Multiple timescales mode-locking mechanism. Our scheme encompasses two scenarios achieved by adjusting the external cavity filter bandwidth. Left: A single MRR resonance within the external cavity filter bandwidth, generating nanosecond pulse trains. Right: Multiple MRR resonances within the filter bandwidth, leading to the generation of pulse burst trains. By driving the phase modulator with a frequency-modulated signal (4.4 MHz modulation, 24.35 GHz carrier signal) generated by an RF synthesizer, we establish a fixed phase relationship among the external cavity modes and MRR resonance, which have free-spectral ranges $F_{\text{ext}} = 4.4$ MHz and $F_{\text{MRR}} = 48.7$ GHz, respectively. The resultant frequency signal is centered at 48.7 GHz, while the spacing between the modulation components resonating inside the external laser cavity is equal to 4.4 MHz.

such as those of a single MRR resonance within filter bandwidth. In the same experimental conditions, Figs. 3(d)–3(f) demonstrate the presence of the picosecond timescale dynamics along with the nanosecond pulses described above due to the phase-locking among

the MRR resonances driven by the GHz modulation. Figure 3(d) shows the generated pulse train acquired using an optical sampling oscilloscope. The measured pulse dynamics exhibit a repetition rate of 48.7 GHz, aligning precisely with the free-spectral range of the MRR. The corresponding temporal pulse width is determined using intensity autocorrelation measurements, as illustrated in Fig. 3(e), the profile of which reveals a sech pulse shape with a width of 3.1 ps and a time-bandwidth product of 0.46. The features corresponding to this timescale remain absent in the radio frequency power spectrum [Fig. 3(c)] due to the bandwidth limitation of the photodiode. We exclusively apply our mode-locking technique to the TM polarization modes of the MRR in the cases illustrated in Figs. 3(d)–3(f), since these modes exhibit a higher parametric gain of 3.1 dB compared to 2.3 dB for the TE modes. Moreover, the TM polarization modes have lower dispersion than the TE modes, leading to a broadening of the optical bandwidth and reduced pulse widths. These characteristics contribute to a more efficient FWM in the pulse burst train regime.⁴² The parametric gain values were obtained by solving the coupled-wave equations within the framework of the nonlinear Schrödinger equation for degenerate FWM, considering an intracavity peak power of 0.56 W. In this regime, our device exhibits a maximum average output power of 8.5 mW, achieved by increasing the cavity gain through the EDFA. This capability renders our laser cavity amenable to micromachining and micro-drilling applications.⁴⁶ The output becomes unstable beyond this power threshold, aligning with the behavior observed in standard fiber mode-locked lasers. One could explore optimization strategies

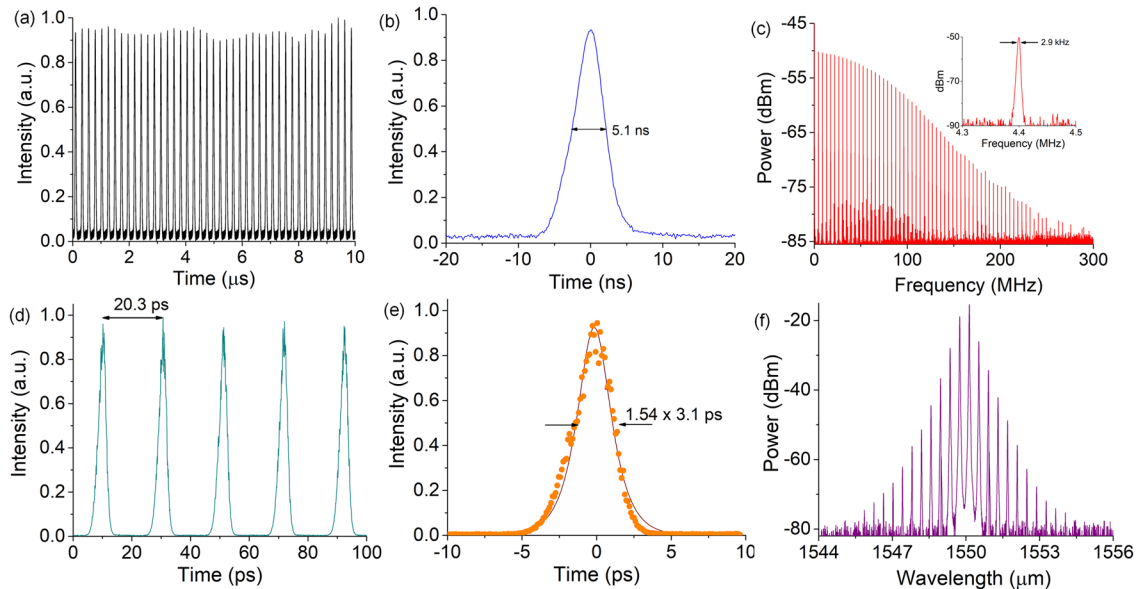


FIG. 3. The mode-locked regime with multiple timescales: The temporal and spectral profiles of coexisting nanosecond and picosecond timescales, with 8.5 mW average output power, for a 100 GHz filter bandwidth. This corresponds to two MRR resonances, the center wavelength being 1549.3 nm. (a) Nanosecond pulse train and (b) a single nanosecond pulse featuring a Gaussian temporal profile of 5.1 ns width, recorded using the photodiode and the real-time oscilloscope. (c) RF spectrum of the trace, indicating a fundamental repetition rate of 4.4 MHz. The inset displays the fundamental RF tone measured with a resolution of 2.9 kHz. (d) Time trace showing a train of pulses with a repetition rate of 48.7 GHz, recorded using the optical sampling oscilloscope. (e) Corresponding autocorrelation trace of the pulse. The width, measured using an autocorrelator (orange dots), is 3.1 ps, perfectly overlapping a sech function profile (brown solid line). (f) The optical spectrum of the multiple timescale mode-locked regime shows a frequency comb.

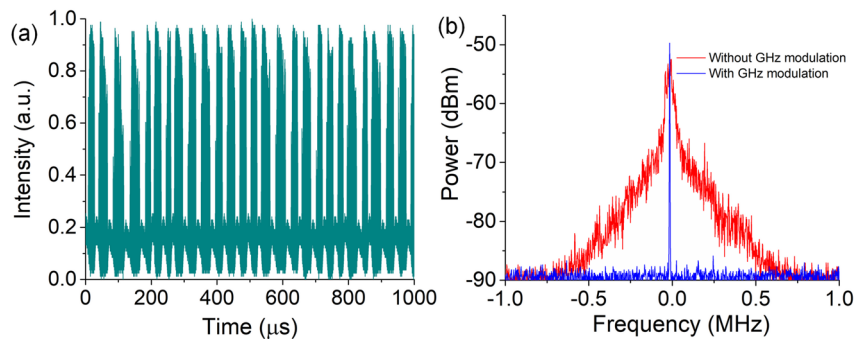


FIG. 4. Effect of GHz modulation. (a) Incoherent beating among the pulses without modulation. (b) Broadening of the RF spectrum in the absence of modulation, resulting in a linewidth of ~ 0.4 MHz (red spectrum). Modulation (blue spectrum) was obtained in the same regime as in Fig. 3, resulting in a narrower linewidth of 2.9 KHz.

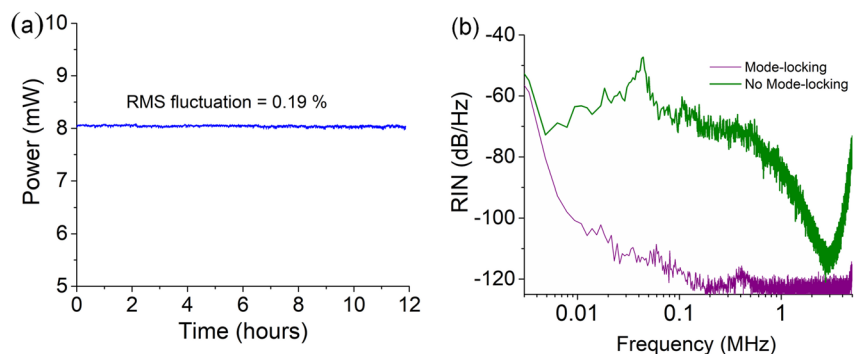


FIG. 5. Stability characterization of the mode-locked operation obtained in the same experimental conditions, as shown in Fig. 3. (a) Power stability measurement over 12 h, presenting a low RMS fluctuation of 0.19% and proving the robustness of operation. (b) RIN characterization of the laser with nanosecond and picosecond components, with (purple) and without (green) mode-locking.

such as dispersion management and external optical amplifiers to enhance the output power further.⁴⁷

Without GHz modulation, the pulse train cannot be phase-locked, resulting from the superposition of multiple independent nanosecond pulses from each MRR resonance. Consequently, incoherent beating among the pulses arises, as shown in Fig. 4(a). Such a beating is also proven by the broadening of the RF spectrum when modulation is absent (red line), with a linewidth of ~ 0.4 MHz, in contrast to the case in which modulation is instead present (blue line), as reported in Fig. 4(b).

Switching from pulse burst trains to solely nanosecond pulse timescales is achieved by reducing the external cavity filter bandwidth to 50 GHz, which allows the transmission of only a single MRR resonance. In this regime, we adjusted the EDFA gain to 11 dB, achieving laser emission with pulses of 1.7 nJ energy and a mode-locking threshold as low as 28 mW. Furthermore, our mode-locking operations are highly stable and robust against noise, resulting in over 12 h of stable output with root-mean-square fluctuations of 0.19% [see Fig. 5(a)] when both timescales coexist. To further validate this claim, we experimentally measured the system relative intensity noise (RIN), a significant performance parameter used to characterize pulse-to-pulse energy variations of mode-locked

lasers.⁴³ The RIN characteristics of the laser with and without active mode-locking are compared in Fig. 5(b), showing >40 dB improvements in the intensity fluctuation among the two cases within the 1 MHz frequency range. Without external frequency modulation, Fig. 6(a) shows the measured spectral profiles achieved with different resonant modes $m = 2, 6$, and 11, corresponding to the passband filter bandwidths of 100, 300, and 550 GHz, respectively. Here, we can observe a broadening of the comb spectra due to FWM, from ~ 1.2 –4.1 nm and 9.2 nm around 1550 nm, corresponding to increasing values of m . We report that the FWM threshold decreases from 120 mW (one single MRR resonance within the filter passband) to 7 mW (two or more MRR resonances within the filter pass-band) as multiple MRR resonances are permitted within the bandwidth, i.e., with a threshold reduction of 17 times. This significant reduction is due to the energy exchange between the nearest MRR resonances, which are, in turn, seeded by the oscillating external cavity modes. Additional increases in MRR resonances do not further lower the threshold, primarily due to energy exchange between the nearest FWM-generated modes. Still, the absence of frequency modulation leads to irregular pulsations in the nanosecond timescale, as illustrated in Fig. 6(b). The autocorrelation trace in Fig. 6(c) for the same operational regime, characterized by

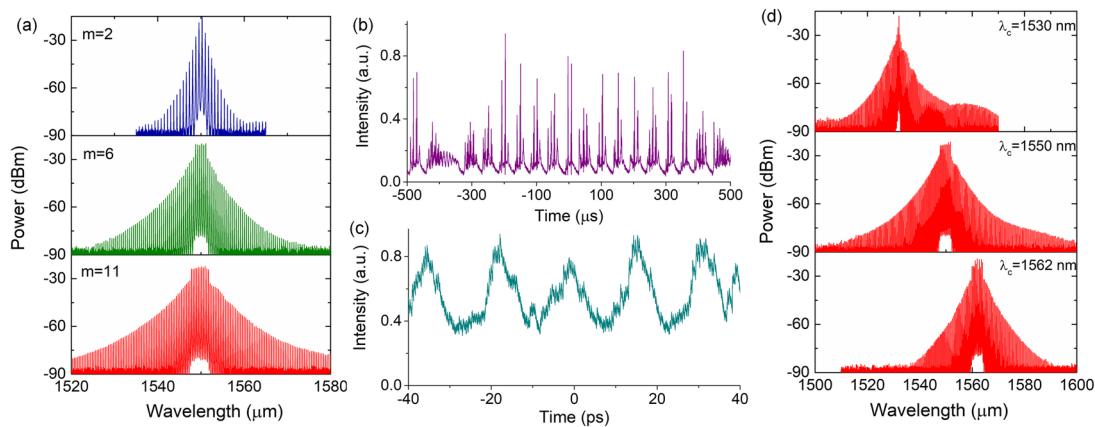


FIG. 6. Laser operation without modulation. (a) Comb spectra were achieved by adjusting the bandwidth of the intracavity filter with different resonant modes $m = 2, 6$, and 11 , corresponding to spectral bandwidths of $100, 300$, and 550 GHz, respectively. We observe that the comb spectra broaden from 1.2 to 4.1 nm and 9.2 nm around 1550 nm for $m = 2, 6$, and 11 , respectively, when considering a 10 dB intensity variation concerning the center comb line, which has the highest intensity. Time-domain characterization in the nanosecond (b) and picosecond (c) timescales, using autocorrelation characterization with a filter bandwidth of 300 GHz. (d) Frequency comb generation obtained by varying the central wavelength of the tunable filter (the bandwidth is fixed at 550 GHz). The observed spectral broadening is $6.0, 9.2$, and 7.8 nm [from top to bottom of (d), respectively] when considering a 10 dB intensity variation with respect to the center comb line, which has the highest intensity.

low contrast autocorrelation, confirms the existence of a fast periodic modulation at 48.7 GHz. These shorter pulses undergo more substantial amplitude modulation, which increases statistical peak power variations.²⁴ Such variations enhance nonlinear interactions and contribute to spectral broadening.^{30,48} On the other hand, in the presence of frequency modulation, the chirp introduced by the PM is partially offset by self-modulation-induced chirp on the propagating pulses, limiting the conversion bandwidth of FWM.⁴⁹ Such uncompensated chirp further contributes to the temporal broadening of the pulses due to cavity dispersion, ultimately reducing peak power and further limiting the efficiency of FWM power transfer between adjacent MRR resonances. Without modulation, there are no such limitations, and the spectrum broadens. This indicates that the dispersion management of the external cavity can lead to generating a broadband comb at femtosecond timescales. As shown in Fig. 6(d), the optical spectrum of the generated frequency comb can be varied by tuning the central wavelength of the bandpass filter (fixed overall filter bandwidth of 550 GHz). The different generated combs have bandwidths of $\sim 6.0, 9.2$, and 7.8 nm, within 10 dB intensity variation, for $\lambda_c = 1530, 1550$, and 1562 nm, respectively.

IV. CONCLUSION

We demonstrate the generation of a highly stable mode-locked laser using an MRR nested in an external optical fiber cavity. We achieve distinct mode-locked regimes characterized by multiple timescales, with nanosecond optical pulses associated with the free-spectral range of the external cavity modes and by the simultaneous presence of picosecond ultra-fast pulses, respectively. The latter reassembles the features of regular pulse burst trains with a spectral profile consistent with the two free-spectral ranges of the external cavity and the MRR at 4.4 MHz and 48.7 GHz REPs, respec-

tively. The nanoseconds (5.1 ns) and picoseconds (3.1 ps) observed timescales correspond to transform limited time-bandwidth products of 0.5 and 0.46 , respectively. Those are achieved above the mode-locked threshold of 28 mW, with a RIN showing ultra-low noise and high long-term stability. By increasing the external cavity filter bandwidth, we can effectively control the transition from a nanosecond to a pulse burst train regime. Dispersion management components can further compress the generated pulses to sub-ps time scales. In the absence of frequency modulation, our configuration facilitates the widening of the spectral bandwidth due to FWM, as two or more MRR resonances exchange energy within the external laser cavity. In this regime, we can adjust the central comb wavelength, offering an extra degree of freedom to support the advancement of applications in frequency-domain spectroscopy, metrology, and dense wavelength division multiplexing for coherent communication.

ACKNOWLEDGMENTS

This work was funded by the Natural Sciences and Engineering Research Council of Canada (NSERC) through the Strategic, Alliance, and Discovery Grants Schemes, by the MESI PSR-SIIRI Initiative in Quebec, and by the Canada Research Chair Program. This work was also supported by the Mitacs Elevate Postdoctoral Fellowship Program. The work of A.V.K. and E.A.V. was supported by the Ministry of Science and Higher Education of the Russian Federation, Research Project No. 2019-1442 (Project Reference No. FSER-2020-0013).

AUTHOR DECLARATIONS

Conflict of Interest

The authors have no conflicts to disclose.

Author Contributions

Aadhi A. Rahim: Conceptualization (equal); Data curation (equal); Formal analysis (equal); Methodology (equal); Resources (equal); Visualization (equal); Writing – original draft (equal). **Imtiaz Alamgir:** Conceptualization (equal); Formal analysis (equal); Investigation (equal); Methodology (equal); Project administration (equal); Validation (equal); Visualization (equal); Writing – original draft (equal); Writing – review & editing (equal). **Luigi Di Lauro:** Conceptualization (equal); Formal analysis (equal); Investigation (equal); Methodology (equal); Project administration (equal); Validation (equal); Visualization (equal); Writing – original draft (equal); Writing – review & editing (equal). **Bennet Fischer:** Conceptualization (supporting); Methodology (supporting); Writing – review & editing (supporting). **Nicolas Perron:** Methodology (supporting); Writing – review & editing (supporting). **Pavel Dmitriev:** Methodology (supporting); Visualization (supporting); Writing – review & editing (supporting). **Celine Mazoukh:** Methodology (supporting); Visualization (supporting); Writing – review & editing (supporting). **Piotr Roztocky:** Conceptualization (supporting); Writing – review & editing (supporting). **Cristina Rimoldi:** Conceptualization (supporting); Visualization (supporting); Writing – review & editing (supporting). **Mario Chemnitz:** Conceptualization (supporting). **Armaghan Eshaghi:** Funding acquisition (supporting); Writing – review & editing (supporting). **Evgeny A. Viktorov:** Writing – review & editing (supporting). **Anton V. Kovalev:** Writing – review & editing (supporting). **Brent E. Little:** Resources (supporting); Writing – review & editing (supporting). **Sai T. Chu:** Resources (supporting); Writing – review & editing (supporting). **David J. Moss:** Writing – review & editing (supporting). **Roberto Morandotti:** Funding acquisition (lead); Resources (lead); Supervision (lead); Writing – review & editing (supporting).

DATA AVAILABILITY

The data that support the findings of this study are available from the corresponding authors upon reasonable request.

REFERENCES

- ¹E. P. Ippen, “Principles of passive mode locking,” *Appl. Phys. B: Lasers Opt.* **58**, 159–170 (1994).
- ²M. Nishiura and T. Shioda, “Wavelength and pulse width programmable mode-locked Yb fiber laser,” *Opt. Express* **31**, 5347–5362 (2023).
- ³A. Aadhi, A. V. Kovalev, M. Kues, P. Roztocky, C. Reimer, Y. Zhang, T. Wang, B. E. Little, S. T. Chu, Z. Wang, D. J. Moss, E. A. Viktorov, and R. Morandotti, “Highly reconfigurable hybrid laser based on an integrated nonlinear waveguide,” *Opt. Express* **27**, 25251 (2019).
- ⁴C. Reimer, S. Sciara, P. Roztocky, M. Islam, L. Romero Cortés, Y. Zhang, B. Fischer, S. Loranger, R. Kashyap, A. Cino, S. T. Chu *et al.*, “High-dimensional one-way quantum processing implemented on d -level cluster states,” *Nat. Phys.* **15**, 148–153 (2019).
- ⁵M. Kues, C. Reimer, P. Roztocky, L. R. Cortés, S. Sciara, B. Wetzel, Y. Zhang, A. Cino, S. T. Chu, B. E. Little, D. J. Moss *et al.*, “On-chip generation of high-dimensional entangled quantum states and their coherent control,” *Nature* **546**, 622–626 (2017).
- ⁶L. Caspani, C. Reimer, M. Kues, P. Roztocky, M. Clerici, B. Wetzel, Y. Jestin, M. Ferrera, M. Peccianti, A. Pasquazi *et al.*, “Multifrequency sources of quantum correlated photon pairs on-chip: A path toward integrated quantum frequency combs,” *Nanophotonics* **5**, 351–362 (2016).

- ⁷P. Roztocky, M. Kues, C. Reimer, B. Wetzel, S. Sciara, Y. Zhang, A. Cino, B. E. Little, S. T. Chu, D. J. Moss, and R. Morandotti, “Practical system for the generation of pulsed quantum frequency combs,” *Opt. Express* **25**, 18940–18949 (2017).
- ⁸C. Reimer, M. Kues, P. Roztocky, B. Wetzel, F. Grazioso, B. E. Little, S. T. Chu, T. Johnston, Y. Bromberg, L. Caspani, D. J. Moss, and R. Morandotti, “Generation of multiphoton entangled quantum states by means of integrated frequency combs,” *Science* **351**, 1176–1180 (2016).
- ⁹C. Reimer, M. Kues, L. Caspani, B. Wetzel, P. Roztocky, M. Clerici, Y. Jestin, M. Ferrera, M. Peccianti, A. Pasquazi, B. E. Little *et al.*, “Cross-polarized photon-pair generation and bi-chromatically pumped optical parametric oscillation on a chip,” *Nat. Commun.* **6**, 8236 (2015).
- ¹⁰X. Xu, M. Tan, B. Corcoran, J. Wu, A. Boes, T. G. Nguyen, S. T. Chu, B. E. Little, D. G. Hicks, R. Morandotti, A. Mitchell, and D. J. Moss, “11 TOPS photonic convolutional accelerator for optical neural networks,” *Nature* **589**, 44–51 (2021).
- ¹¹X. Xu, M. Tan, B. Corcoran, J. Wu, T. G. Nguyen, A. Boes, S. T. Chu, B. E. Little, R. Morandotti, A. Mitchell, D. G. Hicks, and D. J. Moss, “Photonic perceptron based on a Kerr microcomb for high-speed, scalable, optical neural networks,” *Laser Photonics Rev.* **14**, 2000070 (2020).
- ¹²L. Xu, T. F. De Lima, H.-T. Peng, S. Bilodeau, A. Tait, B. J. Shastri, and P. R. Prucnal, “Scalable networks of neuromorphic photonic integrated circuits,” *IEEE J. Sel. Top. Quantum Electron.* **28**, 6101409 (2022).
- ¹³Bennet Fischer, Mario Chemnitz, Yi Zhu, Nicolas Perron, Piotr Roztocky, Benjamin MacLellan, Luigi Di Lauro, A. Aadhi, Cristina Rimoldi, Tiago H. Falk, and Roberto Morandotti, “Neuromorphic Computing via Fission-based Broadband Frequency Generation,” *Advanced Science* **10**, (2023).
- ¹⁴H. A. Haus, “Mode-locking of lasers,” *IEEE J. Sel. Top. Quantum Electron.* **6**, 1173–1185 (2000).
- ¹⁵U. Keller, “Recent developments in compact ultrafast lasers,” *Nature* **424**, 831–838 (2003).
- ¹⁶Bennet Fischer, Mario Chemnitz, Benjamin MacLellan, Robin Roztocky, Benjamin Wetzel, Brent E. Little, Sai T. Chu, David J. Moss, José Azaña, and Roberto Morandotti, “Autonomous on-chip interferometry for reconfigurable optical waveform generation,” *Optica* **8**, 1268–1276 (2021).
- ¹⁷H. Bao, A. Cooper, M. Rowley, L. Di Lauro, J. S. Toterogongora, S. T. Chu, B. E. Little, G.-L. Oppo, R. Morandotti, D. J. Moss, B. Wetzel *et al.*, “Laser cavity-soliton microcombs,” *Nat. Photonics* **13**, 384–389 (2019).
- ¹⁸M. Kues, C. Reimer, B. Wetzel, P. Roztocky, B. E. Little, S. T. Chu, T. Hansson, E. A. Viktorov, D. J. Moss, and R. Morandotti, “Passively mode-locked laser with an ultra-narrow spectral width,” *Nat. Photonics* **11**, 159–162 (2017).
- ¹⁹L. Jin, L. Di Lauro, A. Pasquazi, M. Peccianti, D. J. Moss, R. Morandotti, B. E. Little, and S. T. Chu, “Optical multi-stability in a nonlinear high-order microring resonator filter,” *APL Photonics* **5**, 056106 (2020).
- ²⁰W. Wang, W. Zhang, S. T. Chu, B. E. Little, Q. Yang, L. Wang, X. Hu, L. Wang, G. Wang, Y. Wang, and W. Zhao, “Repetition rate multiplication pulsed laser source based on a microring resonator,” *ACS Photonics* **4**, 1677–1683 (2017).
- ²¹S. Y. Set, H. Yaguchi, Y. Tanaka, and M. Jablonski, “Laser mode locking using a saturable absorber incorporating carbon nanotubes,” *J. Lightwave Technol.* **22**, 51 (2004).
- ²²J. Boguslawski, Y. Wang, H. Xue, X. Yang, D. Mao, X. Gan, Z. Ren, J. Zhao, Q. Dai, G. Soboń, J. Sotor, and Z. Sun, “Graphene actively mode-locked lasers,” *Adv. Funct. Mater.* **28**, 1801539 (2018).
- ²³D. Kim, D. Kwon, B. Lee, and J. Kim, “Polarization-maintaining nonlinear-amplifying-loop-mirror mode-locked fiber laser based on a 3×3 coupler,” *Opt. Lett.* **44**, 1068–1071 (2019).
- ²⁴M. Peccianti, A. Pasquazi, Y. Park, B. E. Little, S. T. Chu, D. J. Moss, and R. Morandotti, “Demonstration of a stable ultrafast laser based on a nonlinear microcavity,” *Nat. Commun.* **3**, 765 (2012).
- ²⁵H. Bao, A. Cooper, S. T. Chu, D. J. Moss, R. Morandotti, B. E. Little, M. Peccianti, and A. Pasquazi, “Type-II micro-comb generation in a filter-driven four wave mixing laser (invited),” *Photonics Res.* **6**, B67–B73 (2018).
- ²⁶R. I. Woodward, E. J. R. Kelleher, T. H. Runcorn, S. Loranger, D. Popa, V. J. Wittwer, A. C. Ferrari, S. V. Popov, R. Kashyap, and J. R. Taylor, “Fiber grating compression of giant-chirped nanosecond pulses from an ultra-long nanotube mode-locked fiber laser,” *Opt. Lett.* **40**, 387–390 (2015).
- ²⁷L. Zenteno, H. Avramopoulos, and G. New, “Detailed analysis of active mode-locking,” *Appl. Phys. B: Photophys. Laser Chem.* **40**, 141–146 (1986).

- ²⁸M. Rowley, B. Wetzel, L. Di Lauro, J. S. T. Gongora, H. Bao, J. Silver, L. Del Bino, P. D. Haye, M. Peccianti, and A. Pasquazi, "Thermo-optical pulsing in a microresonator filtered fiber-laser: A route towards all-optical control and synchronization," *Opt. Express* **27**, 19242–19254 (2019).
- ²⁹A. Pasquazi, L. Caspani, M. Peccianti, M. Clerici, M. Ferrera, L. Razzari, D. Duchesne, B. E. Little, S. T. Chu, D. J. Moss, and R. Morandotti, "Self-locked optical parametric oscillation in a CMOS compatible microring resonator: A route to robust optical frequency comb generation on a chip," *Opt. Express* **21**, 13333–13341 (2013).
- ³⁰A. Pasquazi, M. Peccianti, L. Razzari, D. J. Moss, S. Coen, M. Erkintalo, Y. K. Chembo, T. Hansson, S. Wabnitz, P. Del'Haye, X. Xue, A. M. Weiner, R. Morandotti, P. Del, X. Xue, A. M. Weiner, and R. Morandotti, "Micro-combs: A novel generation of optical sources," *Phys. Rep.* **729**, 1–81 (2018).
- ³¹S. B. Papp, P. Del'Haye, and S. A. Diddams, "Mechanical control of a microrod-resonator optical frequency comb," *Phys. Rev. X* **3**, 031003 (2013).
- ³²G. Pu, L. Zhang, W. Hu, and L. Yi, "Automatic mode-locking fiber lasers: Progress and perspectives," *Sci. China Inf. Sci.* **63**, 160404 (2020).
- ³³B. Zhang, W. Liu, R. Wang, Z. Pan, W. Li, X. Wang, Y. Zhou, E. Xing, J. Tang, and J. Liu, "Thermal effect and application of thermal mode-locking based on optical microsphere cavity," *Opt. Commun.* **530**, 129150 (2023).
- ³⁴H. Herfurth, R. Patwa, T. Lauterborn, S. Heinemann, and H. Pansar, "Micromachining with tailored nanosecond pulses," *Proc. SPIE* **6796**, 67961G (2007).
- ³⁵E. Williams and E. Brousseau, "Simulation and experimental study of nanosecond laser micromachining of commercially pure titanium," *J. Micro Nano Manuf.* **4**, 011004 (2016).
- ³⁶R. A. Martinez, G. Plant, K. Guo, B. Janiszewski, M. J. Freeman, R. L. Maynard, M. N. Islam, F. L. Terry, O. Alvarez, F. Chenard, R. Bedford, R. Gibson, and A. I. Ifarraguerri, "Mid-infrared supercontinuum generation from 16 to $>11\ \mu\text{m}$ using concatenated step-index fluoride and chalcogenide fibers," *Opt. Lett.* **43**, 296–299 (2018).
- ³⁷A. Dutt, C. Joshi, X. Ji, J. Cardenas, Y. Okawachi, K. Luke, A. L. Gaeta, and M. Lipson, "On-chip dual-comb source for spectroscopy," *Sci. Adv.* **4**, 1–10 (2018).
- ³⁸T. Nakamura, J. Davila-Rodriguez, H. Leopardi, J. A. Sherman, T. M. Fortier, X. Xie, J. C. Campbell, W. F. McGrew, X. Zhang, Y. S. Hassan, D. Nicolodi, K. Beloy, A. D. Ludlow, S. A. Diddams, and F. Quinlan, "Coherent optical clock down-conversion for microwave frequencies with 10^{-18} instability," *Science* **368**, 889–892 (2020).
- ³⁹S. B. Papp, K. Beha, P. Del'Haye, F. Quinlan, H. Lee, K. J. Vahala, and S. A. Diddams, "Microresonator frequency comb optical clock," *Optica* **1**, 10–14 (2014).
- ⁴⁰J. Pfeifle, V. Brasch, M. Laueremann, Y. Yu, D. Wegner, T. Herr, K. Hartinger, P. Schindler, J. Li, D. Hillerkuss, R. Schmogrow, C. Weimann, R. Holzwarth, W. Freude, J. Leuthold, T. J. Kippenberg, and C. Koos, "Coherent terabit communications with microresonator Kerr frequency combs," *Nat. Photonics* **8**, 375–380 (2014).
- ⁴¹D. J. Moss, R. Morandotti, A. L. Gaeta, and M. Lipson, "New CMOS-compatible platforms based on silicon nitride and Hydex for nonlinear optics," *Nat. Photonics* **7**, 597–607 (2013).
- ⁴²M. Ferrera, D. Duchesne, L. Razzari, M. Peccianti, R. Morandotti, P. Cheben, S. Janz, D.-X. Xu, B. E. Little, S. Chu, and D. J. Moss, "Low power four wave mixing in an integrated, micro-ring resonator with $Q = 12$ million," *Opt. Express* **17**, 14098 (2009).
- ⁴³C. R. Smith, R. D. Engelsholm, and O. Bang, "Pulse-to-pulse relative intensity noise measurements for ultrafast lasers," *Opt. Express* **30**, 8136–8150 (2022).
- ⁴⁴A. Pasquazi, R. Ahmad, M. Rochette, M. Lamont, B. E. Little, S. T. Chu, R. Morandotti, and D. J. Moss, "All-optical wavelength conversion in an integrated ring resonator," *Opt. Express* **18**, 3858–3863 (2010).
- ⁴⁵L. Di Lauro, J. Li, D. J. Moss, R. Morandotti, S. T. Chu, M. Peccianti, and A. Pasquazi, "Parametric control of thermal self-pulsation in micro-cavities," *Opt. Lett.* **42**, 3407–3410 (2017).
- ⁴⁶M. Kraus, M. A. Ahmed, A. Michalowski, A. Voss, R. Weber, and T. Graf, "Microdrilling in steel using ultrashort pulsed laser beams with radial and azimuthal polarization," *Opt. Express* **18**, 22305–22313 (2010).
- ⁴⁷Y. Wang, J. Li, K. Mo, Y. Wang, F. Liu, and Y. Liu, "14.5 GHz passive harmonic mode-locking in a dispersion compensated Tm-doped fiber laser," *Sci. Rep.* **7**, 7779 (2017).
- ⁴⁸L. Razzari, D. Duchesne, M. Ferrera, R. Morandotti, S. Chu, B. E. Little, and D. J. Moss, "CMOS-compatible integrated optical hyper-parametric oscillator," *Nat. Photonics* **4**, 41–45 (2010).
- ⁴⁹S. A. Planas, N. L. Pires Mansur, C. H. Brito Cruz, and H. L. Fragnito, "Spectral narrowing in the propagation of chirped pulses in single-mode fibers," *Opt. Lett.* **18**, 699–701 (1993).